Segmentation of the left ventricular endocardium from magnetic resonance images by using different statistical shape models

Concetta Piazzese, M. Chiara Carminati, Andrea Colombo, Rolf Krause, Mark Potse, Angelo Auricchio, Lynn Weinert, Gloria Tamborini, Mauro Pepi, Roberto M Lang, et al.

Segmentation of the left ventricular endocardium from magnetic resonance images by using different statistical shape models

Concetta Piazzese[1,2], M. Chiara Carminati[3], Andrea Colombo[1], Rolf Krause[2], Mark Potse[2,4], Angelo Auricchio[2], Lynn Weinert[5], Gloria Tamborini[3], Mauro Pepi[3], Roberto M. Lang[5], Enrico G. Caiani[1]

[1] Dipartimento di Elettronica, Informazione e Bioingegneria, Politecnico di Milano, Italy
[2] Centre for Computational Medicine in Cardiology, Institute of Computational Science, Università della Svizzera italiana, Lugano, Switzerland
[3] Centro Cardiologico Monzino IRCCS, Milan, Italy
[4] Inria Bordeaux Sud-Ouest, Talence, France
[5] Department of Cardiology, University of Chicago, IL, USA

Corresponding author:

Concetta Piazzese
Dipartimento di Elettronica, Informazione e Bioingegneria
Politecnico di Milano, Piazza L. da Vinci 32, Milano, Italy
E-mail: concetta.piazzese@polimi.it

Abstract

We evaluate in this paper different strategies for the construction of a statistical shape model (SSM) of the left ventricle (LV) to be used for segmentation in cardiac magnetic resonance (CMR) images. From a large database of LV surfaces obtained throughout the cardiac cycle from 3D echocardiographic (3DE) LV images, different LV shape models were built by varying the considered phase in the cardiac cycle and the registration procedure employed for surface alignment. Principal component analysis was computed to describe the statistical variability of the SSMs, which were then deformed by applying an active shape model (ASM) approach to segment the LV endocardium in CMR images of 45 patients. Segmentation performance was evaluated by comparing LV volumes derived by ASM segmentation with different SSMs and those obtained by manual tracing, considered as a reference. A high correlation ($r^2 > 0.92$) was found in all cases, with better results when using the SSM models comprising more than one frame of the cardiac cycle.

Key words: Statistical shape model, cardiac MRI, image segmentation, left ventricular volume

1. Introduction

Cardiac magnetic resonance (CMR) is currently the gold standard imaging modality for the assessment of left-ventricular (LV) anatomy and function [1]. Compared to other modalities, main advantages are its non-invasiveness, the ability to modulate tissue contrast in response to several mechanisms and the ability to provide high-quality functional and anatomical images in any anatomical orientation [2].

Real-time cine images, based on steady-state free precession (SSFP) gradient echo sequence acquired with retrospective ECG gating, allow obtaining high-quality 2D images over the cardiac cycle, that are routinely used in clinical practice to evaluate global and regional LV function, including stroke volume, ejection fraction, and wall thickness. In particular, to obtain an estimate of LV volumes and mass, accurate delineation of endocardial and epicardial wall contours on each 2D short-axis (SAX) slice in the acquired stack is required, leading to a time-consuming, tedious, error-prone and subject to intra-operator and inter-operator variability process [3]. Research in this field has been focused in providing methods for increase automatization of the tracing process, without compromising accuracy of the results. Even though processing time has been greatly reduced using different image-based methods [4], the results are still in need of further improvement [5].

To this respect, statistical shape models (SSM) have become a powerful tool to segment medical images [6] by matching a predefined geometric shape to the locations of the extracted image features in a two-step procedure: 1) generating the shape model from a training set; 2) performing the fitting of the model to a new image, thus solving an optimization problem of finding the best model parameters for a given patient image, where instances of the model can only deform in ways found in the training set.

A potential limitation in previous SSM applications [6] to segment the LV from CMR images arises from the fact that the applied 3D shape model used a training set built from manual tracing of 2D SAX CMR slices with anisotropic resolution (1.5 x 1.5 mm planar resolution vs. 6-8 mm slice thickness) subsequently interpolated along the third dimension [7]. In this way, detailed anatomical information along the LV long-axis (typically at LV base and apex) cannot be included in the SSM.

Moreover, potential inter-slice misalignment, if not properly corrected, could introduce errors.

We hypothesized that the utilization of an intrinsically 3D training set, free from misalignment errors, obtained by segmenting the LV endocardium from real-time 3D echocardiographic (3DE) images, could overcome these limitations and be utilized to obtain the 3D SSM for CMR segmentation. In addition, as the anatomical ventricular surface resulting from segmentation would be intrinsically 3D, it could be utilized to directly compute LV volumes (without using methods of disk area sum), as well as to be incorporated in patient-specific models for simulating electro-mechanical cardiac phenomena [8].

Based on these assumptions, we recently proposed an inter-modality statistical modelling approach in which the SSM was built from a first database of about 3000 3D endocardial meshes extracted from transthoracic 3DE images [9] and applied to 12 consecutive patients. Preliminary results showed that, in some cases, due to large shape variations between the surface mesh and LV cross-sections, the matching algorithm failed to attract the mesh surface to the right contour.

Based on these preliminary results, we hypothesized that the performance of the segmentation could depend on the way the 3DE meshes in the databases are composed to generate the model to be deformed. Accordingly, the aim of this work was to study and compare the accuracy of the segmentation of the LV endocardial wall on CMR SAX images using different SSMs, built on different frame selections from the available database, and by applying different alignment criteria with a reference shape.

2. Material and methods

2.1. Shape Model Generation

Compared to our preliminary study [9], the size of the training database was more than doubled by retrospectively including semi-automatically segmented (using commercial software 4D LV-Analysis©, Tomtec) LV surfaces from a total of 435 patients (mean age 51 ± 20 years, 269 males, mean EDV 140 ± 70 ml, mean ESV 73 ± 61 ml, mean EF 52 ± 15 %) with the following pathologies: 293 with normal LV function, 78 with dilated cardiomyopathy, 13 with aortic valve insufficiency, 11 with aortic valve stenosis, 28 with mitral regurgitation and 12 with mitral stenosis. All these patients previously underwent real-time 3DEimaging examination at the University of Chicago, IL, USA or at Centro Cardiologico Monzino, Milan, Italy, approved by IRB in both institutions. In both centres, the same equipment (Philips iE33 with X3-1 probe) and acquisition protocol (wide-angled modality in which wedge-shaped sub-volumes were obtained over four to seven consecutive cardiac cycles during a breath-hold with ECG gating) was utilized. Inclusion criterion in the database was the availability of the segmented 3DE dataset in the hospital information system database, in order to have direct access to the LV surfaces. Consequently, a total of 7010 3D LV endocardial surfaces, each defined by 642 vertices and 1280 faces, was available as training set to generate the shape model.

Custom software for the generation of the SSMs was implemented in Matlab (The MathWorks Inc.). For each mesh, the vertex coordinates corresponding to the positions of three fiducial points (LV apex (AP), mitral (MV), and aortic (AO) valve centres) were used to build a local reference system and to co-register (by roto-translation) the mesh to a randomly chosen LV surface, assumed as reference, by using: 1) the centre of mass (CoM) 2) the AP 3) the plane corresponding to the base

(Figure 1). In this process, scaling was not considered since it is part of the anatomical variability represented by the models.

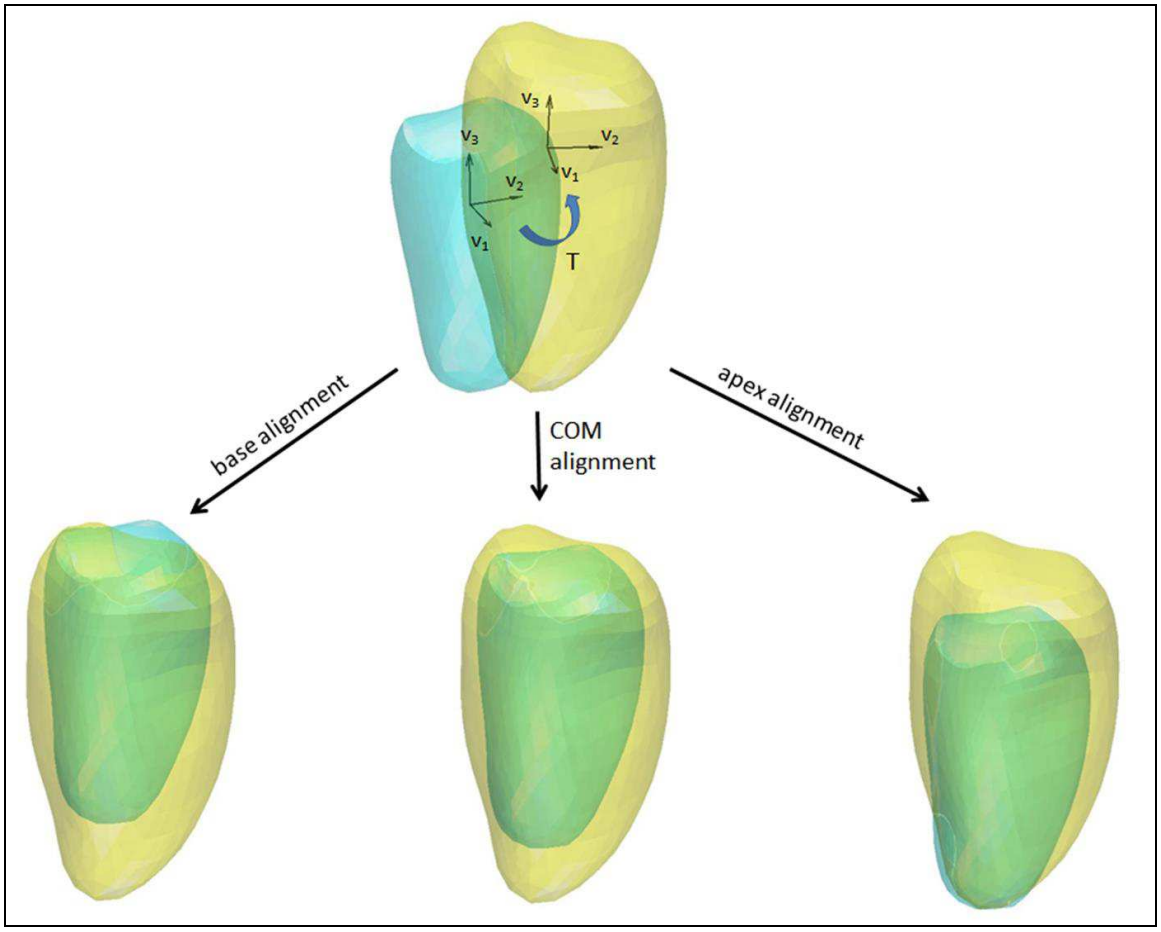

Figure 1. Rotation and translation of a surface (cyan, top) to the reference one (yellow, top). For each of the three alignments, the reference system of each mesh, whom origin is respectively the centre of the plane corresponding to the base, the CoM and the apex, is co-registered to the corresponding reference system of the reference surface.

Four different subsets were created for each of the three possible alignment by selecting the surfaces corresponding to a particular frame in the cardiac cycle: 1) end-diastolic (ED), in which only meshes corresponding to ED frames were considered; 2) end-systolic (ES), in which only meshes corresponding to ES frames were considered; 3) ED-ES, including only meshes corresponding to both ED and ES frames; and 4) global subset, including meshes from all the frames in the cardiac cycle (Figure 2).

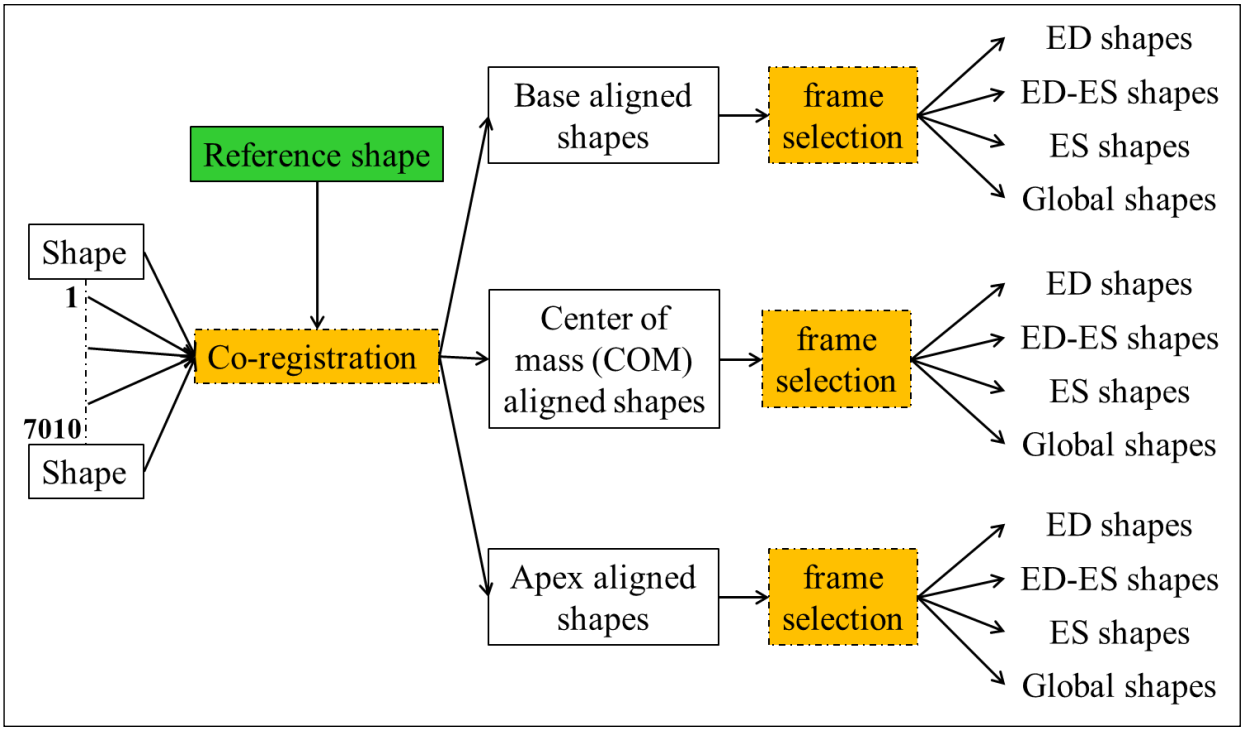

Figure 2. Steps performed to generate different statistical shape models. From the available dataset, 7010 are exported and aligned to three known points (apex, CoM and base) of a reference surface. Each aligned subset of shapes is then analysed for a frame selection so to detect surfaces corresponding to a particular phase of the cardiac cycle.

For each subset, the mean LV endocardial surface is computed by averaging the x, y, z coordinates of the corresponding points of all surfaces. Principal component analysis (PCA) was performed in order to reduce the dimensionality of the subsets and find the minimal number of modes able to describe the variability of each subset [10]. Figure 3 shows the model deformation in each subset using the first and the second principal component (PC). Knowing that cumulative variance is mostly explained by a reduced number of PCs, from 1926 components required to describe the 100% of variability for all models, we constrained the total variability explained to 99.73%, by keeping 74 components for the ED subset, 73 components for the ED-ES subset, 65 components for the ES subset and 70 components for the global subset.

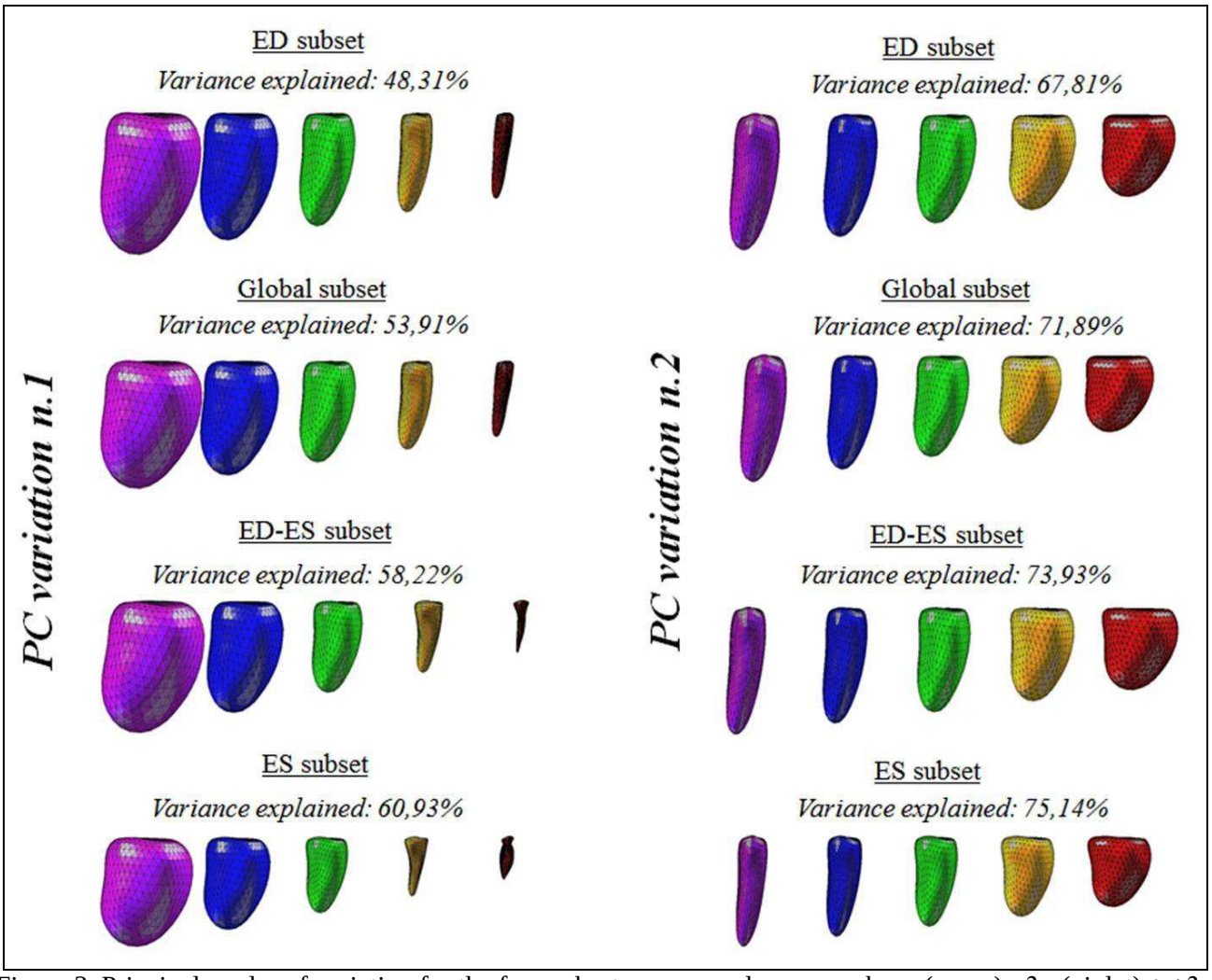

Figure 3. Principal modes of variation for the four subsets, expressed as mean shape (green), -3σ (violet) ÷ +3σ (red), with -1.5σ (blue) and +1.5σ (yellow). In each subset, the first principal component was able to explain about 50% of the total variance, value that increases to about 70% when considering the first two PCs.

2.2. Cardiac Magnetic Resonance Imaging Population

Among patients referred for cardiac evaluation at Centro Cardiologico Monzino, we retrospectively selected CMR datasets considering as inclusion criteria ischemic dilated cardiomyopathy (CMD), coronary artery disease (CAD) and normal LV function. These conditions were selected to include a variety of possible LV size and function in the validation of the proposed method. A total of 45 patients (mean age 60 ± 12 years, 32 males, mean EDV 171 ± 50 ml, mean ESV 93 ± 53 ml, mean EF 49 ± 16 %) were included in this study (15 CMD, 15 CAD and 15 with normal LV function). For each patient, available CMR ECG-triggered multiple 2D images in SAX view (CMR stack) had been acquired using a 1.5 T scanner (Discovery MR450, GE Healthcare, Milwaukee, WI, USA) equipped with an eight element torso coil using a standard cardiac MR protocol based on SSFP gradient echo sequence acquired with retrospective ECG gating. The following sequence parameters were used: echo time 1.57 ms, repetition time 3.2 ms, slice thickness

8 mm, no gap between slices, and pixel size from 0.7 to 1.4 mm. In addition, LAX views (two-, three and four-chamber views) were also available.

2.3. CMR Pre-processing and SSM user initialization

Before segmentation, each CMR stack was pre-processed to compensate for potential spatial misalignments, caused by patient's breath-related motion during image acquisition [11].

In order to properly scale and define the initial position of each mean SSM inside the CMR data, the user was first required to select two points corresponding to the mitral valve (MV) leaflet insertion, and one point corresponding to the LV apex (AP) in both the 2-chambers (2ch) and 4-chambers (4ch) LAX CMR images. An additional point was initialized on the 3-chambers (3ch) LAX CMR image in correspondence to the aortic valve, to properly rotate the initial model. A scale factor was finally computed considering the MV-AP distance in the CMR data and applied to the mean SSM, if inside the possible variations defined by PCA.

2.4. CMR LV segmentation by SSM deformation

Custom software for CMR LV segmentation based on SSM deformation was developed in Matlab (The Mathworks Inc.) and applied to manually selected ED and ES frames. Each scaled mean SSM was iteratively deformed until a stable condition was reached. At each iteration, the SSM is positioned inside the CMR stack (Figure 4A) and deformed according to the grayscale information contained in every 2D SAX plane. (Figure 4B). For detailed algorithm information, please refer to [9]. Briefly, the pixel video intensity profile of the line connecting each intersection point (between the 3D mesh and the 2D image plane) to the centre of mass in a circular region of interest was extracted (Figure 4C). By converting all line profiles to polar coordinates, a radial image (Figure 5A) was then obtained, in which the endocardial position was detected by k-means clustering followed by morphological operators (see Figure 5 for details) and transformed back in Cartesian coordinates (Figure 6A). In particular, a different number of clusters (k=3 for apical slices and k=5 for mid and basal slices), depending on the position of the analysed SAX plane (1/3 apical, 1/3 mid, 1/3 basal) in respect to the total number of planes acquired, was applied.

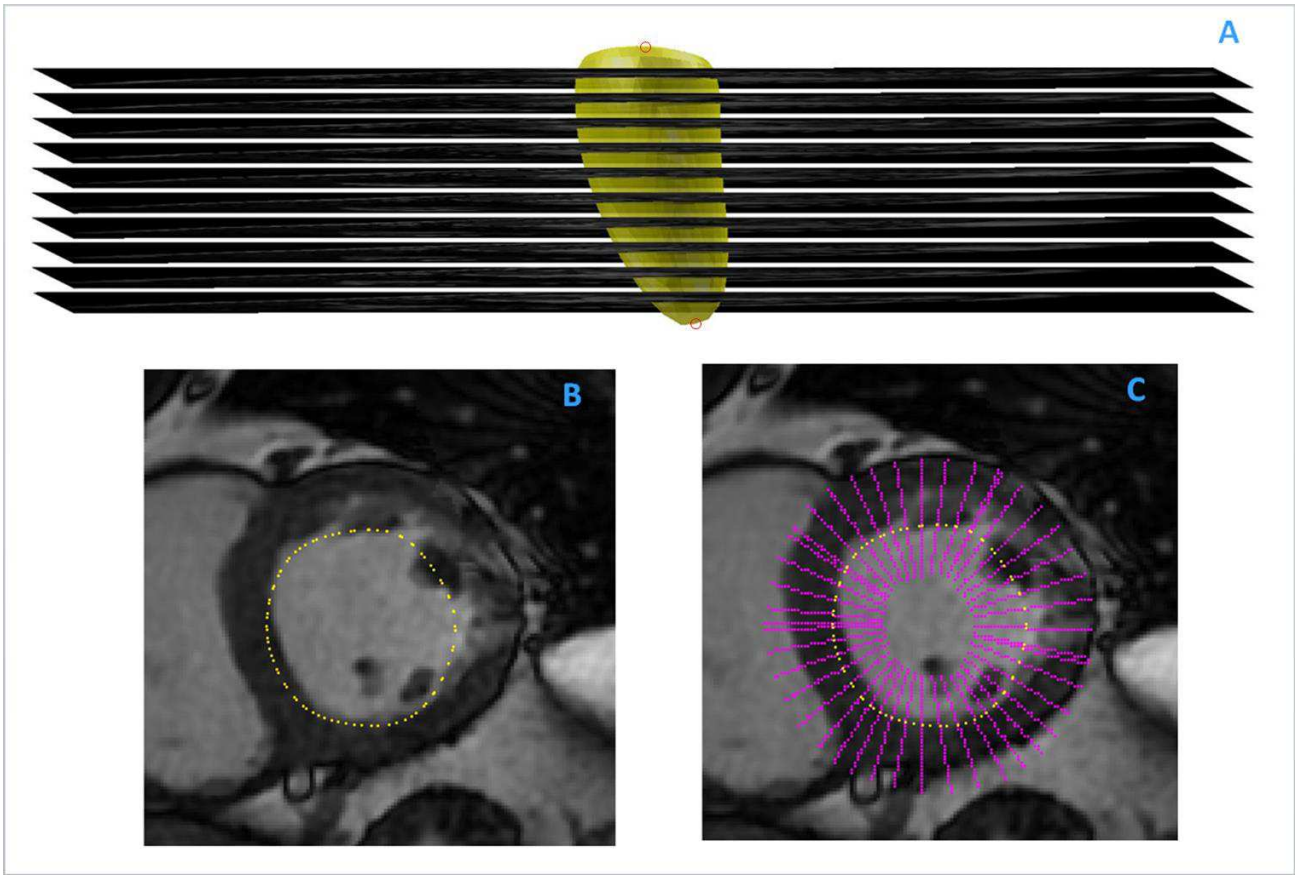

Figure 4. The six-points manually placed on both LAX images are used to compute the average positions of MV centre and AP (red circles) and to correctly pose the mean shape inside the stack of SAX images (A). During the deformation process, the intersection points between the model and each plane are computed (B) along with lines (magenta) connecting each intersection points to the centre of mass in a circular region of interest (C).

To include the papillary muscles in the LV cavity (Figure 6A, green arrows), blood-tissue interface detected points were processed to find smallest convex set containing them (Figure 6B). These points were then used as LV endocardial candidate nodes in the iterative process to update the SSM.

Once the previous steps were applied to all the SAX planes in the CMR stack, a displacement vector for each node, based on the position of the respective candidate points, was computed (Figure 6C) and the 3D SSM globally deformed to match simultaneously all candidate points position. Model variations are controlled by restricting the shape deformations in the range ($-3\sigma \div +3\sigma$) of the PCs selected during each SSM creation.

The active shape modelling (ASM) approach here described was iterated until the resulting SSM mean displacement was less than the planar resolution in the SAX images (Figure 6D). Finally, 3D LV endocardial volume was computed as the sum of volumes of all the regular triangular patches composing the 3D LV mesh. Furthermore, the 2D contours obtained as intersections of the final 3D LV mesh with each SAX plane were used to computed LV volumes using disc-area summation method (modified Simpson's rule), as done routinely in clinical practice.

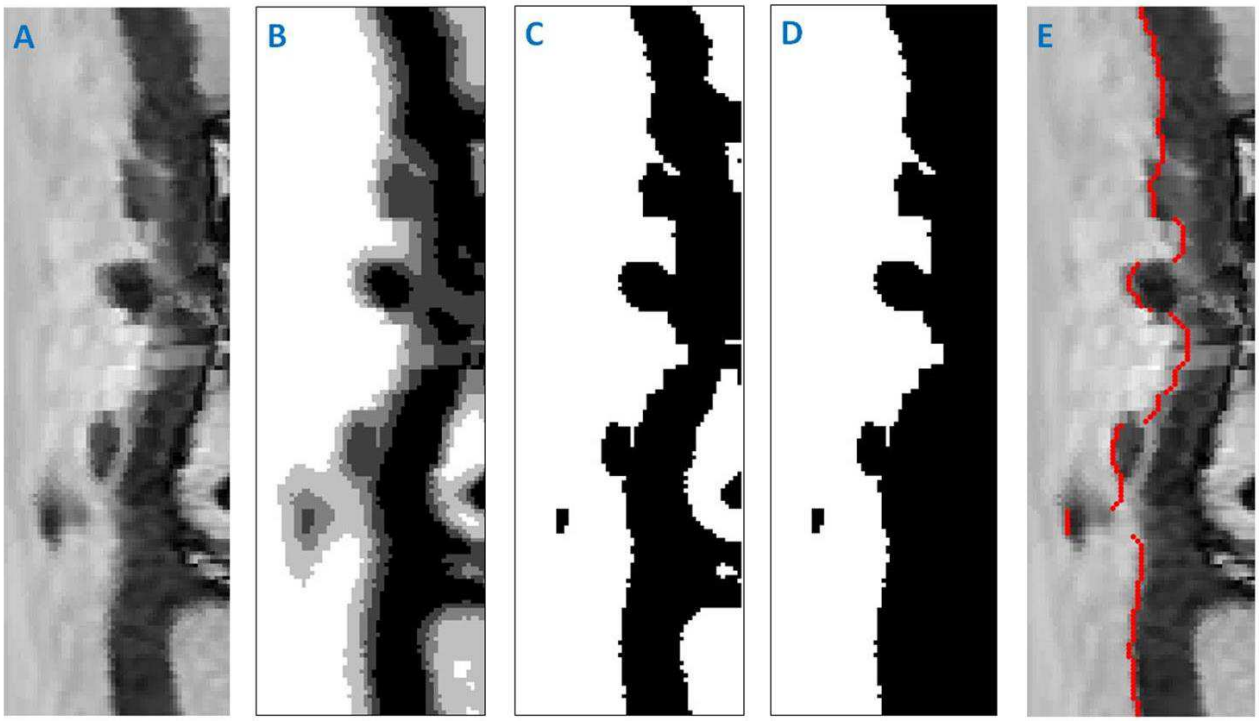

Figure 5. Different steps of the SAX segmentation process. (A) Radial image, created by transforming line video intensity profiles from Cartesian to polar coordinates; (B) Clustered image with a number of cluster equal to 5; (C) Image binarization with a threshold; (D) removal of external structures; (E) Segmented endocardial edge (red) superimposed the initial radial image;

2.5 Gold standard analysis

For each CMR dataset, ED and ES frames were visually selected and the LV endocardial contours manually traced by an expert operator using custom software (open source visualization toolkit – VTK. End-diastolic and ES volumes were obtained by disc-area summation method (modified Simpson's rule) and used as 'gold standard' (GS) for comparison. Papillary muscles were included in the ventricular cavity. If basal SAX images contained both ventricular and atrial myocardium, slices were considered to be part of the LV if the blood cavity in the axial plane was surrounded by 50% or more of ventricular myocardium and the contours were drawn to the junctions between atrium and ventricle and joined by a straight line through the blood pool [12].

2.6. Statistical analysis

For each CMR stack, all the 12 generated SSMs (4 models with 3 different alignments) were applied to the ED and the ES frames. In addition, SSMs generated from the 3DE ED frame subset and SSMs generated from the 3DE ES frame subset were used to segment respectively CMR ED and ES images, to test the effect of generating the model with specific cardiac phase dependence in the training set. Also, the number of iterations required by the deformation process to converge was

considered for each SSM.

Linear correlation and Bland-Altman analysis were used to compare GS volumes to both 3D model volumes, and volumes computed from 2D contours as disc-summation. Two-way ANOVA with repeated measures on both factors (alignment and frame-selection) was used to test differences between LV volumes obtained using the 15 different strategies analysed. Differences in 3D volumes among frame-specific models were evaluated using one-way analysis of variance for correlated samples and Tukey HSD test for multi-comparison correction. The number of iterations required by the model deformation process to converge was evaluated by median and interquartile difference.

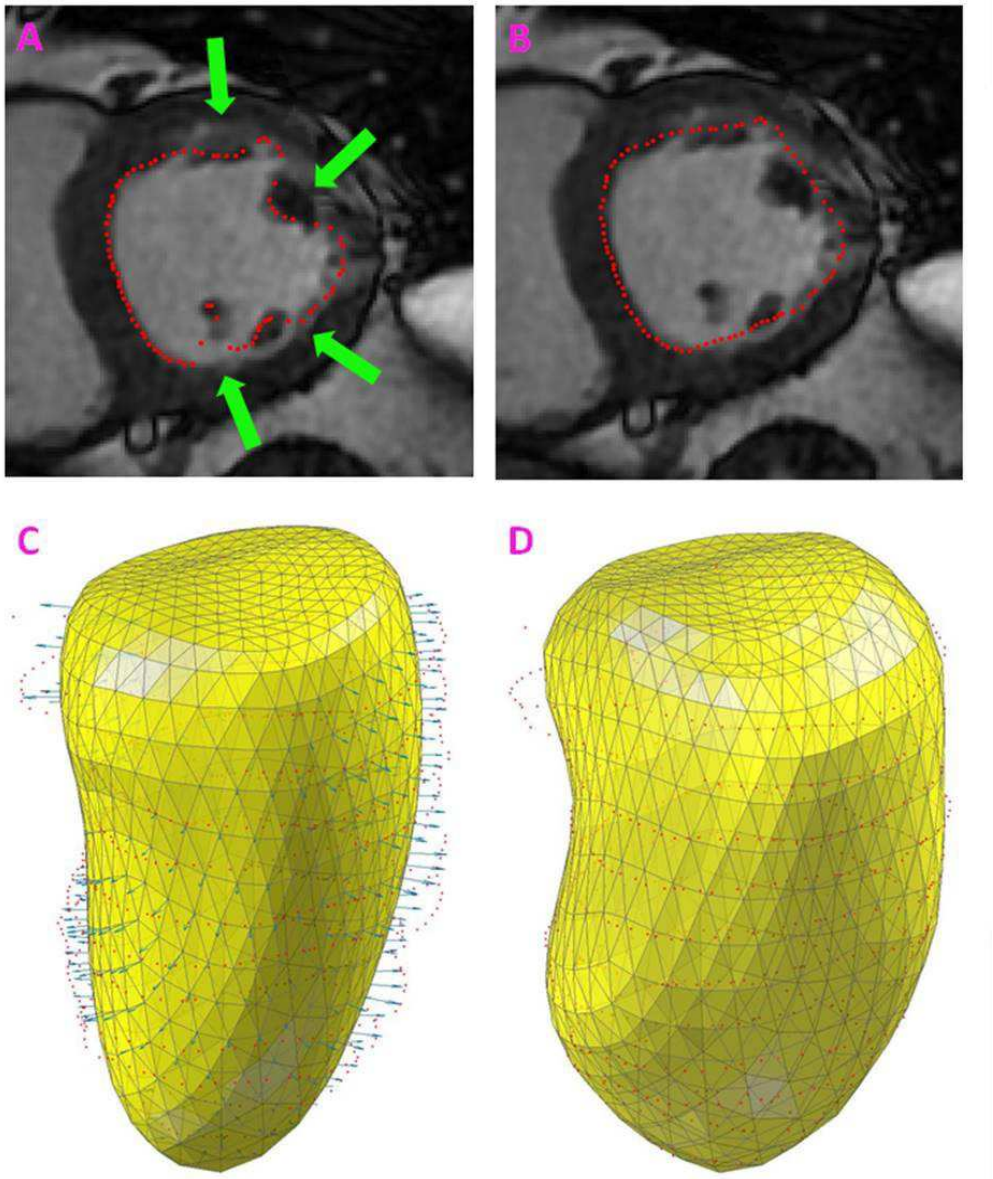

Figure 6. Detected endocardial points are transformed back to Cartesian coordinates on the SAX plane (A). In order to include papillary muscle in the LV cavity (green arrows), each set of interface points is evaluated so to find the smallest convex set that contains it (B). Pixel positions detected at the border of the convex hull

were used to globally deform the initial SSM (C) and match the LV endocardial position in all SAX planes simultaneously. The iteration process continues to modify the model until a stable condition is reached (D).

3. Results

Each model was successfully applied in all the 45 patients. The segmentation process required around 1 minute for each CMR stack using a conventional laptop (Intel_Core i5 2.5 GHz, 8 GB RAM).

Figure 7 shows two examples of the results of the segmentation using the model built using ED and ES frames, superimposed as contours at intersections with the SAX planes on the ED frames (left) and as 3D meshes in LAX (right) views at both ED (top) and ES (bottom) frames. Even if the model is deformed based on the intersections of the SSM with the SAX planes only, it is possible to visually appreciate the correspondence of the detected surface to the LV endocardial position also in both 2- and 4-chamber views, as well as the visual anatomical correspondence at LV apex and base levels.

Correlation analysis (Table 1) showed similar results in all the 15 configurations analysed, with slopes close to unity and high correlation coefficients when GS volumes were compared with 3D SSM volumes (r^2 from 0.92 to 0.96) or with volumes obtained from the 2D segmented contours (r^2 from 0.92 to 0.94). Bland–Altman analysis showed, compared to the GS, an overestimation (bias = 0.25 ÷ 5.2 ml) for 3D meshes and an underestimation for volumes obtained from 2D contours (bias = -5.9 ÷ -2.9 ml), with relatively narrow limits of agreement in both cases corresponding to a range of -28 ÷ 34 ml for 3D meshes and -39 ÷ 29 ml for volumes obtained with the disk's summation rule.

Two-ways ANOVA revealed no significant differences between volumes when segmenting the LV using a model aligned to the centre of mass, to the AP or to the plane corresponding to the base of a reference surface. However, some difference in volumes was present according to the different frame selection in the training set, with a significant interaction between alignment and frame-selection ($p < 0.05$). Specifically, one-way ANOVA showed that the frame selection in the training set could influence the volumetric result ($p < 0.01$), in particular when choosing ES frames, thus resulting in significant underestimation compared to all the other frame selections. Tukey HSD test found no significant difference between ED-ES model, global model and frame-specific model. The model created using only ED frames showed no differences only with the ED-ES model while ES model revealed significance in volumes when compared to the other models.

Iterations to convergence were very similar for each strategy with a median value of 5 and interquartile difference of 0, except the ED model that had an interquartile difference equal to 1 (Table 1, right).

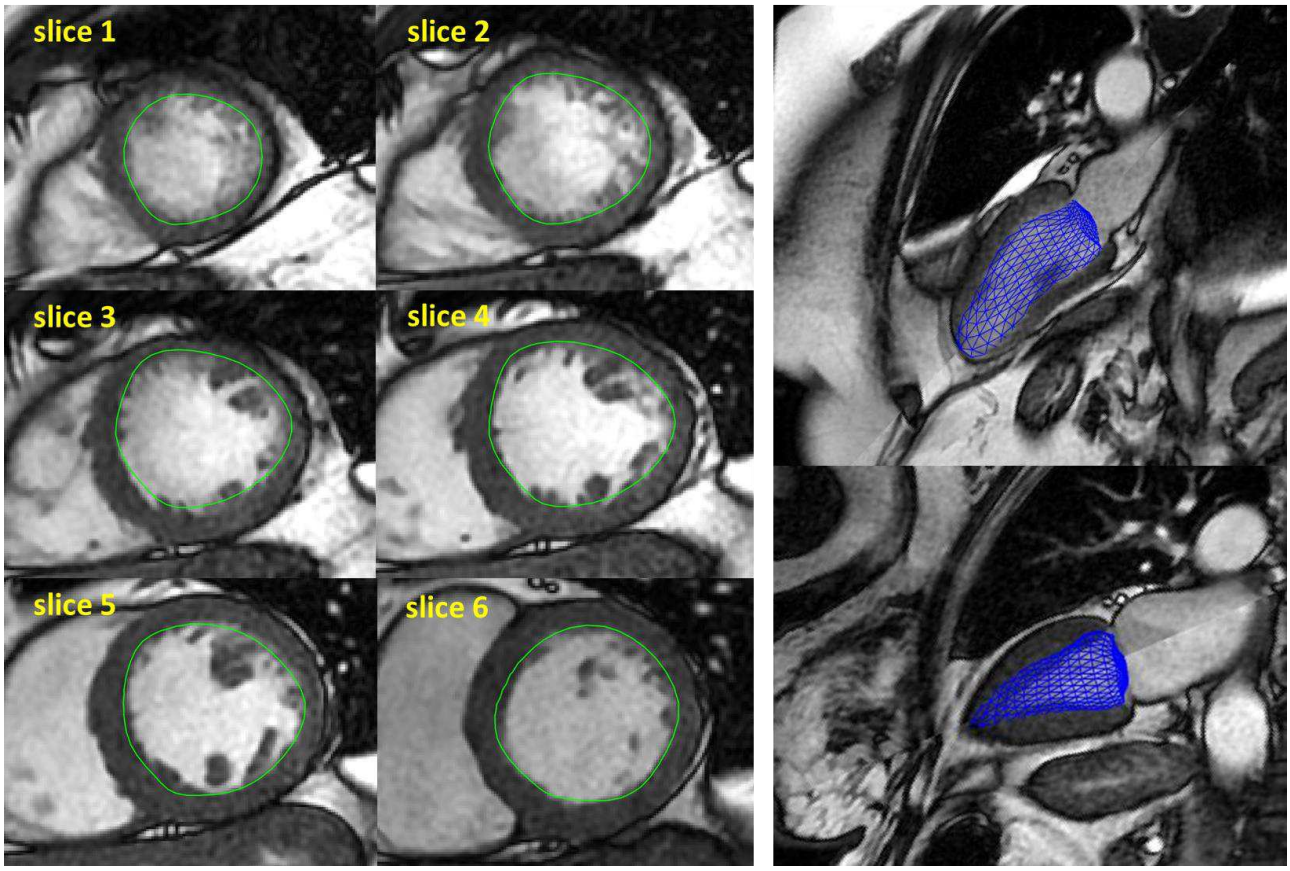

Figure 7. Left: examples of contours (green) obtained as intersections of the final 3D LV deformed model with each ED SAX plane. Right: examples of the final 3D mesh (blue) superimposed on ED (top) and ES (bottom) LAX views.

4. Discussion

We studied the accuracy and performance of the LV endocardial segmentation in SAX CMR images by applying different 3D SSMs of the LV using ASM. All models were built starting from the same database of 3DE LV endocardial surfaces, but including a different frame selection and a different alignment strategy to generate the training set.

This study extends our previous results [9] by utilizing a larger (more than doubled) training databased and by testing the different SSMs on a larger patient population.

In terms of ASM model generation, in comparison to the utilization of training datasets obtained using CMR images, 3DE allows to obtain not interpolated and intrinsically 3D LV endocardial surfaces, resulting in an ASM consistent with LV anatomy, in particular in the representation of LV apex and base at the level of the mitral plane. Compared to the utilization of computed tomographic images, temporal resolution of 3DE is higher, allowing a large number of frames to be obtained from each subject, or a better frame selection for inclusion in the training set. In addition, 3DE imaging technique has the advantage of being widely used and non-invasive, without contraindications in patients with implanted devices, without the need for longer apneas during acquisitions that could affect CMR image quality, thus providing the potential for further expanding the training dataset to

different patients' groups of larger size.

			3D VOLUMES			3D VOLUMES (Simpson's rule)			# iteration	
			r^2	bias [ml]	±1.96σ [ml]	r^2	bias [ml]	±1.96σ [ml]	median	Interquartile difference (3rd – 1st)
alignment	base	ED model	0.94	5.8 (*)	-25 ÷ 36	0.92	-4.5	-40 ÷ 31	5	1
		ED-ES model	0.96	5 (*)	-22 ÷ 32	0.93	-4.5	-40 ÷ 31	5	0
		ES model	0.95	2.4	-26 ÷ 31	0.93	-5.9 (*)	-40 ÷ 28	5	0
		Global model	0.95	3.9	-25 ÷ 33	0.94	-4.8	-38 ÷ 28	5	0
		Frame-specific model	0.96	4 (*)	-22 ÷ 30	0.94	-5.1 (*)	-37 ÷ 27	5	0
	apex	ED model	0.95	5.6 (*)	-24 ÷ 35	0.92	-4	-40 ÷ 32	5	0
		ED-ES model	0.96	5.6 (*)	-21 ÷ 33	0.93	-3.8	-37 ÷ 29	5	1
		ES model	0.94	1.1	-31 ÷ 34	0.93	-5.7 (*)	-41 ÷ 29	5	0
		Global model	0.94	5.4 (*)	-25 ÷ 36	0.93	-4.1	-39 ÷ 31	5	0
		Frame-specific model	0.96	4 (*)	-24 ÷ 32	0.93	-4.5	-39 ÷ 30	5	0
	CoM	ED model	0.95	6.1 (*)	-23 ÷ 36	0.93	-2.9	-38 ÷ 32	5	0
		ED-ES model	0.96	4.5	-21 ÷ 30	0.93	-3.8	-38 ÷ 30	5	0
		ES model	0.95	2	-25 ÷ 29	0.93	-4.9 (*)	-39 ÷ 30	5	1
		Global model	0.96	3.9 (*)	-23 ÷ 30	0.94	-4.4	-36 ÷ 27	5	0
		Frame-specific model	0.96	4.6 (*)	-20 ÷ 30	0.94	-4 (*)	-35 ÷ 27	5	0

Table 1. Statistical analysis to evaluate the segmentation accuracy of fifteen SSM approaches. Linear correlation and Bland-Altman analyses were used to compare the 3D SSM volumes, computed as the sum of volumes of all the regular triangular patches composing the 3D mesh, as well as of 2D contours of the model, obtained on SAX images at the final iteration, with volumes computed from gold standard 2D manual tracings. Also, the number of iterations required by the deformation process of each model to converge were reported. CoM, centre of mass. *: $p<.01$, semi-automatic volumes vs GS.

In comparison to our work, Bai et al. [13] used real 3D cine balanced SSFP CMR datasets (1.25 × 1.25 × 2mm), obtained from a large (> 1000) number of healthy volunteers, and semi-automated segmentation to obtain 3D biventricular meshes on which to build an atlas for its utilization in both SSM, statistical motion model and statistical parametric mapping. The availability of this kind of imaging modality, not conventional in clinical practice, overcome the limitation of constructing a SSM from cine 2D CMR, similar to what we performed by choosing 3DE as source of imaging. By comparison of the amount of variability related to the first two PC modes reported by Bai (44% and 17%, respectively), it is possible to observe very similar results with our SSM (see Figure 3). However, the SSM model of Bai et al. [13] is representative of normal LV morphology only, as input datasets were all from normal subjects, due to intrinsic limitation of 3D CMR imaging that required 20-25 sec apnea, not achievable in pathologic population. In addition, besides describing the model creation, no results of validation in applying it to a testing group of 2D CMR data are present in [13], thus precluding direct comparison with our segmentation result accuracy.

With the proposed approach, independently of the SSMs used to segment the LV endocardium, results are provided both as 3D model, suitable to be easily integrated to into a patient-specific model for electromechanical simulation and analysis [14], and as 2D LV contours on the original SAX images in order to compute the LV volume by traditional formulas. Obtained results showed high correlation ($r^2 > 0.92$) with the GS independently from the strategy utilized. As expected, there was a trend to overestimate or underestimate the LV volumes when computed from the 3D resulting mesh or by 2D disc-area summation, respectively. This difference could be due to the more defined anatomy in the 3D mesh of the base and the apex of the LV, structures not completely visible when considering the 2D CMR stack, thus affecting inclusion of slices in the volume computation.

Considering separately ED and ES volumes, subdividing the population into the three pathologic groups, or by range of EF, once expressing the SD of the Bland-Altman analysis as error % instead than in ml, dependency of the results with the size of the LV was found, independently of the strategy adopted for generating the SSM. In particular, the best accuracy in segmentation was reached once LV size was bigger (i.e., at ED in the DCM group where EF < 40%, with SD = 4% - 5%), while worst results were achieved in NL with EF > 50% at ES (SD = 18% - 22%). Intermediate and size dependent results were present in the CAD group, mainly characterized by EF between 40% and 50%. This trend in segmentation algorithm performance could explain the apparent big SD once results are given as relevant to the whole population.

The different modalities of shape alignment (to the base, to the CoM or to the apex of a reference surface) during the creation of the initial SSM seemed not to influence volumes computation after 3D segmentation. On the contrary, in agreement with other studies, the selection of the frame in the generation of the SSM plays a fundamental role, as it can affect the results of the segmentation. Paragios et al. [15] used a linear combination of the systolic and the diastolic shapes and projected the computed shape to the desired image features, thus extracting endocardial boundaries in echocardiographic apical views. Zhu et al. [16] created a subject-specific dynamical model that simultaneously handles temporal dynamics (intra-subject variability) and inter-subject variability in order to predict the specific cardiac dynamics based on the shapes observed in past frames. In our work, models created including more than one specific frame of the cardiac cycle showed a greater variability that advantaged the segmentation accuracy of the LV endocardium in all subjects, compared to the GS. Similar results were obtained using the ED-ES model, the global model and the frame-specific model. This could be due to the large number of subjects included in the training datasets (7010 frames) covering a large morphological variability. As it could be expected, dissimilarities were obtained for the SSM built from the ED frames and the SSM build from the ES frames only, that showed a lower capability to deform when applied to segment respectively CMR images in the ES frames and in the ED frames.

Some limitations of our previous work [9] were here overcome, by building SSMs from a larger training dataset (specifically, 59 patients with dilated cardiomyopathy and 171 patients with normal LV function were added) that included LV morphology from different patient groups (i.e. extremely dilated, with LBBB) that enabled segmentation of different pathological patients.

A potential limitation of this study is that our approach did not consider the training of a dedicated grey level or intensity model, as it is usually performed in active appearance model (AAM) algorithms [17]. Mitchell et al. [18] showed a successful application of AAM in two substantially different cardiac imaging modality (MR and echocardiographic images). In our case, the construction and the deformation of the SSMs was guided only by shape constraints not taking advantage of all the

available information. This choice was made in order to avoid the need for intensity model retraining, which would have required further manual analysis on CMR images. Another limitation is that we did not apply independent component analysis (ICA), that delivers statistically independent projections of the training samples, in combination with PCA to construct SSMs and to perform LV detection. Different works [19, 20] showed that, since PCs modes represent the global shape variability in the training set and ICA modes highlight local variations, the combination of PCA and ICA could improve the segmentation in 2D cardiac images.

Finally, it was not possible to directly compare results of 3D volumes, as the utilized GS was based on manual tracings on 2D images, from which volumes were computed as disk summation.

6. Conclusion

We evaluated the accuracy of different strategies to obtain SSMs from a large training set of LV surfaced obtained from 3DE, in order to segment the LV endocardium and obtain LV volumes in CMR images, using an inter-modality statistical modelling approach.

We used more than 7000 3D LV endocardial surfaces extracted from 3DE images from a heterogeneous cohort of patients as training datasets, and different strategies for model generation were investigated. The models obtained by considering more than one frame of the cardiac cycle resulted in LV volumes with higher agreement with the manual GS-derived volumes, compared to models built a single-frame selection for the training set. In general, the choice of registering each mesh to the centre of mass, to the AP or to the plane corresponding to the base of a reference LV surface for the initial alignment did not have effect on segmentation accuracy.

The use of a 3D SSMs allowed accurate segmentation of the LV endocardial walls, with a realistic anatomical delineation of both the apex and the base of the LV, thus resulting in a realistic LV morphology that could be utilized also for patient-specific modelling purposes.

Acknowledgements

This work was supported by the Italian Space Agency (contract number 2013-032-R.0, recepient E.G.C.).

References

[1] Pattynama PMT, De Roos A, Van der Wall EE, Van Voorthuisen AE. Evaluation of cardiac function with magnetic resonance imaging. Am Heart J 1994;128:595–607.

[2] Bogaert J, Dymarkowski S, Taylor AM. Clinical cardiac MRI. New York: Springer; 2012.

[3] Lu Y, Radau P, Connelly K, Dick A, Wright G. Segmentation of left ventricle in cardiac cine MRI: An automatic image-driven method. Funct. Imag. Model. Heart, pp. 339–347, 2009.

[4] Albà X, Figueras I Ventura RM, Lekadir K, Tobon-Gomez C, Hoogendoorn C, Frangi AF. Automatic cardiac LV segmentation in MRI using modified graph cuts with smoothness and interslice constraints. Magn Reson Med. 2014 Dec;72(6):1775-84. doi: 10.1002/mrm.25079.

[5] Mahnken AH, Mühlenbruch G, Koos R, Stanzel S, Busch PS, Niethammer M, Günther RW, Wildberger JE. Automated vs. manual assessment of left ventricular function in cardiac multidetector row computed tomography: comparison with magnetic resonance imaging. Eur Radiol. 2006 Jul;16(7):1416-23.

[6] Heimann T, Meinzer HP. Statistical Shape Models for 3D Medical Image Segmentation: A Review. Medical Image Analysis, Vol. 13, No. 4, pp. 543-563, 2009.

[7] Boehler T, Boskamp T, Mueller H, Hennemuth A, Peitgen HO. Evaluation of Active Appearance Models for Cardiac MRI. In Proc. BVM, pages 171–175. T. Tolxdorff, 2006.

[8] Lopez-Perez A, Sebastian R, Ferrero JM. Three-dimensional cardiac computational modelling: methods, features and applications. BioMedical Engineering OnLine. 2015;14:35. doi:10.1186/s12938-015-0033-5.

[9] Caiani EG, Colombo A, Pepi M, Piazzese C, Maffessanti F, Lang RM, Carminati MC. 3D Left ventricular segmentation from MRI images for patient-specific modeling purposes. Europace 2014;16(suppl_4):iv96-101iv

[10] Cootes TF, Cooper D, Taylor CJ, Graham J. A trainable method of parametric shape description. Image Vis Comput 1992;10:289–94.

[11] Carminati MC, Maffessanti F, Caiani EG. Nearly automated motion artifacts correction between multi breath-hold short-axis and long-axis cine CMR images. Comput Biol Med 2014;46:42–50.

[12] Alfakih K, Plein S, Thiele H, Jones T, Ridgway JP, Sivananthan MU. Normal human left and right ventricular dimensions for MRI as assessed by turbo gradient echo and steady-state free precession imaging sequences. J Magn Reson Imaging. 2003 Mar;17(3):323-9.

[13] Bai W, Shi W, de Marvao A, Dawes TJ, O'Regan DP, Cook SA, Rueckert D. A bi-ventricular cardiac atlas built from 1000+ high resolution MR images of healthy subjects and an analysis of

shape and motion. Med Image Anal. 2015 Sep 1;26(1):133-145.

[14] Xia L, Huo MM, Wei Q, Liu F, Crozier S. Analysis of cardiac ventricular wall motion based on a three.-dimensional electromechanical biventricular model. Phys. Med. Biol., vol. 50, pp.1901 -1917 2005.

[15] Paragios N, Jolly M P, Taron M and Ramaraj R. Active shape models and segmentation of the left ventricle in echocardiography. Proc. Scale Space and Pde Methods in Computer Vision, 2005, vol 3459 pp 131–42.

[16] Zhu Y, Papademetris X, Sinusas AJ, Duncan JS. Segmentation of the left ventricle from cardiac MR images using a subject-specific dynamical model. IEEE Trans Med Imaging, 2010, 29(3): 669–687.

[17] Leung KYE, Stralen MV, Burken GV, Jong ND, Bosch JG. Automatic active appearance model segmentation of 3D echocardiograms. Proceedings of ISBI, Rotterdam, Netherlands, 2010, pp. 320–323.

[18] Mitchell S, Bosch J, Lelieveldt B, van der Geest R, Reiber J, Sonka M. 3-D active appearance models: segmentation of cardiac MR and ultrasound images. IEEE Trans. Med. Imaging 21 (9), 2002, 1167–1178.

[19] Uzumcu M, Frangi AF, Reiber JHC, Lelieveldt BPF. Independent component analysis in statistical shape models. In: Proceedings of SPIE medical imaging, 2003, vol 5032, pp 375–383

[20] Koikkalainen J, Lötjönen J. Image segmentation with the combination of the PCA- and ICA-based shape models. In: IEEE International Symposium on Biomedical Imaging: From Nano to Macro, 2004. pp. 149–152